

Coordinated Strategies in Realistic Air Combat by Hierarchical Multi-Agent Reinforcement Learning

1st Ardian Selmonaj
IDSIA, USI-SUPSI
Lugano, Switzerland
ardian.selmonaj@idsia.ch

2nd Giacomo Del Rio
IDSIA, USI-SUPSI
Lugano, Switzerland
giacomo.delrio@idsia.ch

3rd Adrian Schneider
Armasuisse S+T
Thun, Switzerland
adrian.schneider@armasuisse.ch

4th Alessandro Antonucci
IDSIA, USI-SUPSI
Lugano, Switzerland
alessandro.antonucci@idsia.ch

Abstract—Achieving mission objectives in a realistic simulation of aerial combat is highly challenging due to imperfect situational awareness and nonlinear flight dynamics. In this work, we introduce a novel 3D multi-agent air combat environment and a *Hierarchical Multi-Agent Reinforcement Learning* framework to tackle these challenges. Our approach combines heterogeneous agent dynamics, curriculum learning, league-play, and a newly adapted training algorithm. To this end, the decision-making process is organized into two abstraction levels: low-level policies learn precise control maneuvers, while high-level policies issue tactical commands based on mission objectives. Empirical results show that our hierarchical approach improves both learning efficiency and combat performance in complex dogfight scenarios.

Index Terms—Multi-Agent Reinforcement Learning, Hierarchical Policies, Curriculum Learning, Air Combat Simulation.

I. INTRODUCTION

Reinforcement Learning (RL) has demonstrated remarkable potential in complex decision-making tasks. Its effectiveness is exemplified by Lockheed Martin’s work [1], where an RL agent outperformed human pilots in simulated air combat scenarios, establishing it as a notable milestone in the field. Multi-agent dogfighting, a close-range aerial battle between fighter aircraft, involves rapid maneuvers, high-speed engagements, and precise coordination. Its inherent complexity arises from partial observability, nonlinear dynamics, and adversarial interactions. This makes dogfighting a highly challenging domain for *Multi-Agent Reinforcement Learning* (MARL) research, requiring precise control and high-level tactical reasoning.

To address these challenges, we develop a custom 3D multi-agent air combat environment that integrates the JSBSim flight dynamics model [2], enabling physically accurate and aerodynamically precise simulation of aircraft behavior. To effectively learn complex maneuvers, we consider a *Hierarchical MARL* (HMARL) approach by structuring decision-making across *two* levels of abstraction. Low-level policies handle continuous aircraft control, while high-level policies issue tactical commands guiding strategic course of actions and engagement decisions. This hierarchical structure supports structured and explainable reasoning, facilitating the emergence of complex aerial tactics. We further incorporate *heterogeneous* agents to reflect diverse capabilities and operational roles found in real-world engagements. In summary, our main contributions are:

- we present a realistic air combat environment suitable for MARL simulations under heterogeneous dynamics;
- we introduce an effective HMARL framework to learn advanced strategies in competitive aerial engagements;
- we adapt the recently introduced *Simple Policy Optimization* (SPO) [3] algorithm to the multi-agent domain;
- we empirically validate our model to advocate the advantages of our design choices. Our code is publicly available at: anonymous.science/AirCombatHMARL.

II. RELATED WORK

We focus explicitly on *multi-agent* RL methods in 3D air combat environments, while the survey [4] also includes *single-agent* RL and 2D dynamics. Several existing works employ techniques that are relevant to multi-agent air combat, such as tactical reward shaping [5], heterogeneous agents [6], attention-based neural networks for situational awareness [7], or communication mechanisms [8] to improve mission strategies. *Curriculum Learning* (CL) with gradually increasing task difficulty is applied in [9], while enhanced coordination among agents is achieved by adapted training algorithms [10].

The application of HMARL in defense contexts is comparatively limited. An HMARL approach that employs attention mechanisms and self-play is introduced in [11]. Frameworks more closely related to ours appear in [12], [13], with the former integrating CL and the latter employing heterogeneous leader-follower agents together with JSBSim.

In this work, we introduce a complex 3D air combat environment and a training framework to learn hierarchical policies using reward shaping and cascaded league-play that gradually increases mission complexity under realistic and heterogeneous conditions. In contrast to prior efforts that are built on established RL algorithms such as *Proximal Policy Optimization* (PPO) [14], we additionally adapt the recently presented SPO algorithm [3] to the hierarchical multi-agent domain. To the best of our knowledge, this adapted setup has not yet been studied in this context and represents a significant step toward enhancing the realism of such applications.

III. PRELIMINARIES

A. Multi-Agent Reinforcement Learning

MARL involves $n \in \mathbb{N}$ agents learning in a shared environment. We model the agent interactions as a *Partially*

Observable Markov Game (POMG) [15], defined by \mathcal{G}_m as:

$$\mathcal{G}_m := (\mathcal{N}, \mathcal{S}, \{\mathcal{A}^i\}_{i=1}^n, \{\mathcal{O}^i\}_{i=1}^n, \{O^i\}_{i=1}^n, P, \rho, \{R^i\}_{i=1}^n, \gamma),$$

where, $\mathcal{N} = \{1, \dots, n\}$ is the set of agents, \mathcal{S} is the state space, \mathcal{A}^i the action space of agent $i \in \mathcal{N}$, with $\mathcal{A} = \prod_{i=1}^n \mathcal{A}^i$ being the joint action set, \mathcal{O}^i is the set of possible agent observations, while $O^i : \mathcal{S} \rightarrow \Delta(\mathcal{O}^i)$ is the agent's observation function with probability simplex $\Delta(\cdot)$, $P : \mathcal{S} \times \mathcal{A} \rightarrow \Delta(\mathcal{S})$ is the state transition kernel, $\rho \in \Delta(\mathcal{S})$ is the initial state distribution, $R^i : \mathcal{S} \times \mathcal{A} \times \mathcal{S} \rightarrow \mathbb{R}$ is the reward function of agent i , and $\gamma \in [0, 1)$ controls the effect of future rewards.

At each time step $t \in \mathbb{N}$, let the random variable S_t describe the state of the game. Starting from an initial state $s_0 \sim \rho$, each agent i receives a local observation $o_t^i \sim O^i(\cdot | s_t)$ and selects an action $a_t^i \in \mathcal{A}^i$ according to its individual policy $\pi^i(a | o_t^i)$. The joint action $\mathbf{a}_t = (a_t^1, \dots, a_t^n) \in \mathcal{A}$ is drawn from the joint policy $\pi(\mathbf{a}_t | \mathbf{o}_t) = \prod_{i=1}^n \pi^i(a_t^i | o_t^i)$. The POMG transitions to a new state according to $s_{t+1} \sim P(s_{t+1} | s_t, \mathbf{a}_t)$, and each agent i receives a reward $R^i(s_t, \mathbf{a}_t, s_{t+1})$. Each agent aims to maximize its expected discounted return:

$$V^i(s) := \mathbb{E}_{P, O, \pi} \left[\sum_{t=0}^{\infty} \gamma^t R^i(S_t, \mathbf{A}_t, S_{t+1} | S_0 = s) \right]. \quad (1)$$

B. Hierarchical Multi-Agent Reinforcement Learning

HMARL uses temporal abstraction by breaking the overall task into a hierarchy of sub-tasks, which improves learning efficiency [16]. Abstract hierarchical commands, called an *option*, invoke a control policy for a limited duration. Within a lower level, the same option can be applied to control similar aircraft, which supports generalization and alignment with hierarchical structures of defense organizations. Our hierarchical system is modeled as a *Partially Observable Semi-Markov Game* (POSMG) [17], given as:

$$\mathcal{G}_s := (\mathcal{N}, \mathcal{S}, \{\mathcal{C}^i\}_{i=1}^n, \{\mathcal{Z}^i\}_{i=1}^n, \{Z^i\}_{i=1}^n, \mathcal{P}, \rho, \{\mathcal{R}^i\}_{i=1}^n, \gamma),$$

with $\mathcal{N}, \mathcal{S}, \rho, \gamma$ as for \mathcal{G}_m , while the new components are: \mathcal{C}^i , the set of temporally extended high-level actions (options) available to agent i . Each option $c \in \mathcal{C}^i$ is a triple $c = (\mathcal{I}_c, \pi_c, \beta_c)$, with initiation set $\mathcal{I}_c \subseteq \mathcal{S}$, intra-option controller π_c (being a low-level policy from \mathcal{G}_m), and termination condition $\beta_c : \mathcal{S} \rightarrow [0, 1]$. The observation function is $Z^i : \mathcal{S} \rightarrow \Delta(\mathcal{Z}^i)$, where \mathcal{Z}^i is the observation space. The semi-Markov transition kernel over next states and option duration is given by $\mathcal{P} : \mathcal{S} \times \mathcal{C} \rightarrow \Delta(\mathcal{S} \times \mathbb{N}_+)$, with joint option set $\mathcal{C} = \prod_i \mathcal{C}^i$. The cumulative reward is given by $\mathcal{R}^i : \mathcal{S} \times \mathcal{C} \times \mathcal{S} \times \mathbb{N}_+ \rightarrow \mathbb{R}$. At each decision epoch $(t_k, k) \in \mathbb{N}$ with random durations $\tau_k = t_{k+1} - t_k \in \mathbb{N}_+$, agent i observes $z_{t_k}^i \sim Z^i(\cdot | s_{t_k})$ and selects an option according to its high-level policy $c_{t_k}^i \sim \pi_h^i(\cdot | z_{t_k}^i)$, which activates one of the low-level policies $\{\pi_{c_{t_k}^i}^j\}_{j=1}^n$ to execute primitive-time actions $a_t \sim \pi_{c_{t_k}^i}(\cdot | o_t)$ in the underlying POMG until at least one option terminates according to $\{\beta_{c_{t_k}^i}^j\}_{j=1}^n$ after duration τ_k . The state evolves as $(s_{t_{k+1}}, \tau_k) \sim \mathcal{P}(\cdot | s_{t_k}, c_{t_k})$ and a cumulative reward $\mathcal{R}^i(s_{t_k}, c_{t_k}, s_{t_{k+1}}, \tau_k)$ is distributed to each agent. The objective is to maximize the expected return (1).

IV. METHOD

A. Environment

Air combat scenarios are generally categorized into *beyond visual range* and *within visual range* engagements. Here, we focus on the latter, that is the relevant scenario for dog-fighting. Realistic aircraft physics is essential for competitive performance. Therefore, we built a custom training environment using JSBSim, an open-source flight dynamics simulator based on real-world physics and control systems. An effective MARL process requires careful design of agent interactions, state-action spaces, reward structures, and scalability to capture mission dynamics. In our environment, the state space includes the aircraft's geographic position (x, y, z) [m], velocity v [m/s], acceleration \dot{v} [m/s²], relative distance to opponents d [m], *Aspect Angle* (AA) ω_a [°], *Antenna Train Angle* (ATA) ω_t [°], and heading angle ω_h [°] (Fig. 1a). All scalar values of state variables are normalized to the range $[-1, 1]$ and concatenated to a vector. The action space is different for each hierarchy level and presented in the following. Cannon fire, i.e., an unguided kinetic weapon, is modeled using a *Weapon Engagement Zone* (WEZ), in which an agent has an 80% probability of being destroyed per simulation step. The WEZ covers a range of 3.5 km and an angular span of 8° (Fig. 1b). Missiles are excluded, as their long range and guidance capabilities could negate the purpose of close-range engagements for dogfighting.

As real-world combat scenarios often involve diverse aircraft types, we consider an heterogeneous setup involving the established F16 Fighting Falcon and Douglas A4 Skyhawk models. The F16 is a supersonic, highly maneuverable fighter, whereas the A4 Skyhawk is a subsonic aircraft with lower top speed but excellent handling at low altitudes. We keep the WEZ constant for both aircraft, while their differing flight dynamics are realistically simulated through JSBSim, which runs at a physics integration frequency of 100 Hz, i.e., $\delta t = 0.01$ seconds are simulated per environment step.

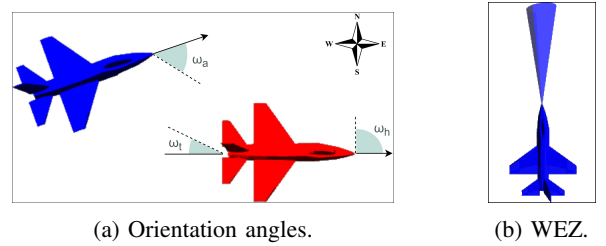


Fig. 1: Aircraft postures showing: (a) attacking angles, and (b) cannon fire modeled through the WEZ.

B. Low-Level Control Policies

Low-level policies are responsible for steering the aircraft, of which we define three types in the following. The actions $a_t^i \in \mathcal{A}^i = [0, 1]^4$ of each agent i include the maneuver controls: *i*) aileron (roll), *ii*) elevator (pitch), *iii*) rudder (yaw), *iv*) throttle for power management, and *v*) a shoot command for

cannon fire. Their observation o_t^i contains information about themselves and their nearest enemy aircraft. They constitute the intra-option controllers π_c of \mathcal{G}_s to be selected by the high-level policy π_h . Based on domain knowledge, we restrict our framework to a small set of low-level policies, which revealed to be a reasonable design choice as they reflect core tactical maneuvers in real-world engagements, where simplicity and robustness are favored over an overly diverse action set. Similar low-level policies are also considered by [1] and [18].

1) *Engage*: The engage policy π_e aims to achieve an advantageous position by placing the agent behind the enemy, pointing towards it while the enemy is oriented straight ahead. Let ω_r denote the roll angle. We model deviations from optimal values $\omega_a = \omega_t = \omega_r = 0$ as Gaussian functions:

$$b_a := e^{-\left(\frac{\omega_a}{10^\circ}\right)^2}, \quad b_t := e^{-\left(\frac{\omega_t}{10^\circ}\right)^4}, \quad b_r := e^{-\left(\frac{\omega_r}{25^\circ}\right)^2}. \quad (2)$$

Function b_t has a steeper slope to emphasize the importance of positioning behind the enemy. Similarly, the distance component b_d decreases if the agent is outside shooting range:

$$b_d := \begin{cases} e^{-\left(\frac{d-3.5 \text{ km}}{10 \text{ km}}\right)^2}, & \text{if } d > 3.5 \text{ km}, \\ 1, & \text{if } d \leq 3.5 \text{ km}. \end{cases} \quad (3)$$

The total posture reward is defined as the smoothed product:

$$r_p := \sqrt{b_a \cdot b_t \cdot b_r \cdot b_d} \in [0, 1]. \quad (4)$$

With an additional event reward $r_e := -5$ for crashing or being destroyed by the opponent, an altitude penalty $r_a := -1$ for falling below a safety altitude of 3 km, and a shooting penalty $r_s := -0.5$ per shot, the total per-step reward for π_e is

$$r_{\pi_e} := r_s + r_e + r_a + 0.05 \cdot r_p \in [-6.5, 0.05]. \quad (5)$$

2) *Attack*: The attack policy π_a aims to aggressively destroy the enemy. We model the kill reward based on the positioning at the moment the enemy is destroyed, i.e., the more the agent attacks from behind, the higher the reward:

$$r_k := (g_{1,10} \circ \cos)(\omega_t) = 4.5 \cos(\omega_t) + 5.5 \in [1, 10], \quad (6)$$

where $g_{a,b}(\cdot)$ is a range transformation function that shifts the original range to $[a, b]$. We also include a slightly relaxed posture reward to encourage the agent to approach the enemy:

$$r_o := \sqrt{b_a \cdot b_r \cdot b_d} \in [0, 1]. \quad (7)$$

The final per-step reward used to train π_a is given by:

$$r_{\pi_a} := r_k + r_e + r_a + 0.01 \cdot r_o \in [-6, 10.01]. \quad (8)$$

3) *Defend*: The defend policy π_d aims to evade opponents by maintaining a large distance from them. To achieve effective evasive behavior, we use a potential reward:

$$r_d := \Phi(s_{t+1}) - \Phi(s_t), \quad \Phi(s_t) := \frac{d(s_t)}{d_m}, \quad (9)$$

where $d(s_t)$ is the distance to the enemy at state s_t , and $\Phi(s_t)$ is normalized by the map size d_m . Therefore, r_d is positive only if the distance at the new state s_{t+1} is larger than at the previous state s_t . The total per-step reward for π_d is:

$$r_{\pi_d} := r_s + r_e + r_a + r_d \in [-6.5, 0.1]. \quad (10)$$

C. High-Level Commander Policy

The *commander* policy π_h determines which low-level policy each agent will use. The observations $z_{t_k}^i$ include information about *i*) the calling agent i , *ii*) its two closest opponents, and *iii*) its nearest friendly aircraft. The option set is $\mathcal{C}^i := \{0, 1, 2\}$, $i \in \mathcal{N}$, where $c_{t_k} = 0$ activates π_d , $c_{t_k} = 1$ activates π_e , and $c_{t_k} = 2$ activates π_a . The selected low-level policy π_c then receives the corresponding observation o_t^i . While the commander has no direct control over the agent's steering maneuvers, it is responsible for deciding an effective course of actions for its low-level policies. We keep the reward structure simple, allowing π_h to autonomously discover an optimal strategy. The only components are the *kill* reward (6) (with range $g_{1,5}$) and the event penalty $r_e = -5$, accumulated over option duration τ_k . Thus, the total reward for π_h is:

$$r_{\pi_h} := r_e + r_k \in [-5, 5]. \quad (11)$$

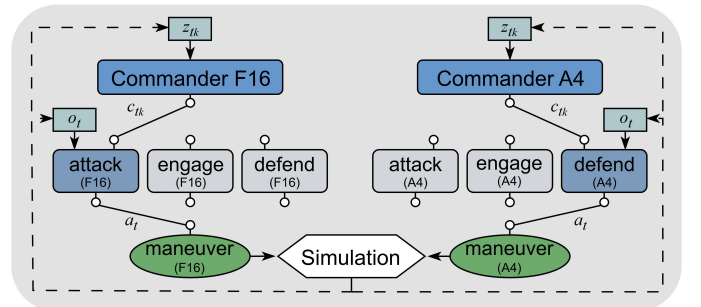


Fig. 2: Hierarchical simulation process: for each aircraft type, a shared commander policy decides which low-level policy to activate, this in turn producing control maneuvers.

D. Curriculum Learning and League-Play

In our framework, we employ shared policies for each aircraft type, i.e., all F16 agents use the same instances of the low-level policies π_a , π_e , and π_d , as well as the same commander instance π_h (Fig. 2). The same also applies to A4 agents. For convenience, we abbreviate F16 with the superscript (f) and A4 with (a). Consequently, there are six low-level policies to learn: $\pi_c \in \{\pi_a^f, \pi_e^f, \pi_d^f, \pi_a^a, \pi_e^a, \pi_d^a\}$, and two high-level policies: $\pi_h \in \{\pi_h^f, \pi_h^a\}$.

The learning process starts with training low-level policies. We adopt a CL scheme with levels by transferring the policy to the next level once training completes. Level complexity increases by making opponents more competitive. We first train a simple tracking aircraft to follow random pre-set locations, similar to π_e but with reduced observation and action spaces, denoted π_0 . The enemy behavior according to CL levels are: *L1*) π_0 with random targets, *L2*) π_0 targeting the agent with slight disturbances and manual cannon fire, *L3*) self-play, where the agent engages against itself, and *L4*) league-play, where each control policy π_c is trained against mixed opponent behaviors, i.e., in each episode, opponents are randomly assigned any π_c from L3. This final stage L4 further improves engagement capabilities and prepares

agents for diverse opponent strategies. Once low-level training completes, we train high-level policies π_h with π_c fixed as options. CL is no longer required, since low-level skills are already established and the focus shifts to coordinating them strategically. Instead, π_h faces opponents with a mixed strategy over the L4 policies: π_a (40%), π_e (40%), and π_d (20%), thereby encouraging competitive adversary behavior.

E. Learning Algorithm

We adopt Actor-Critic neural networks [19], where the actor models the policy π with parameters θ and the critic, with parameters ϕ , learns the value function defined in (1). The network architecture is identical across all policies (except for observation and action spaces) and designed as follows: (i) two linear layers of size 200 with tanh activation; (ii) an attention module (for situational awareness) of size 200; (iii) the outputs of the three preceding components are added and passed through a normalization layer; and (iv) a final linear output layer of size 200. The hierarchical policies π_h follow the *Centralized Training and Decentralized Execution* (CTDE) [20] paradigm, where the critic has access to the full state s_{t_k} , while the actor operates solely on local observations z_{t_k} .

We employ the SPO algorithm to update network parameters. The SPO surrogate policy loss maintains policy updates within a trust region by penalizing deviations of the probability ratio. Unlike PPO, which can set gradients to zero for some samples by ratio clipping, the SPO loss uses all samples to update the policy toward the trust region. It is defined as:

$$\mathcal{L}_s := -\mathbb{E}_{\pi_{\theta_{old}}} \left[r_t(\theta) \hat{A}_t - \frac{|\hat{A}_t|}{2\epsilon} \cdot (r_t(\theta) - 1)^2 \right], \quad (12)$$

where $r_t(\theta) = \frac{\pi_\theta(a_t|s_t)}{\pi_{\theta_{old}}(a_t|s_t)}$ denotes the probability ratio, ϵ is a hyperparameter, and \hat{A}_t the estimated advantage [21]. The value function loss measures the error between the predicted values $V_\phi(s_t)$ and the target returns \hat{R}_t as follows:

$$\mathcal{L}_v := \mathbb{E}_t \left[\left(V_\phi(s_t) - \hat{R}_t \right)^2 \right]. \quad (13)$$

Finally, an entropy term encourages exploration as follows:

$$\mathcal{L}_e := -\mathbb{E}_{\pi_\theta} [-\log \pi_\theta(a_t|s_t)] = -\mathcal{H}(\pi_\theta). \quad (14)$$

The total actor-critic loss is thus defined as:

$$\mathcal{L} := \mathcal{L}_s + \kappa_v \mathcal{L}_v + \kappa_e \mathcal{L}_e, \quad (15)$$

where κ_v and κ_e are positive coefficients controlling the respective loss regularization terms. A pseudo-code description of the learning process is provided in Algorithm 1, which is used for training all policies π_c and π_h . Since the hierarchical policies π_h employ the CTDE framework, our method represents the first adaptation of the SPO algorithm to the multi-agent setting, which we denote as *Multi-Agent Simple Policy Optimization* (MA-SPO). This extension is motivated by the well-established adaptation of PPO to MA-PPO [14], whose demonstrated effectiveness in various multi-agent domains indicates that a similar adaptation of SPO can likewise achieve a strong performance, which we validate in the next section.

Algorithm 1 Simple Policy Optimization Algorithm

- 1: **Initialize:** policy π_θ and value V_ϕ , hyperparameter ϵ , coefficients κ_v, κ_e , learning rates $\lambda_\theta, \lambda_\phi$
 - 2: **while** not termination condition **do**
 - 3: Collect data $\mathcal{D} = \{(s_t, a_t, r_t)\}_{t=1}^M$ using policy π_θ
 - 4: Set $\pi_{\theta_{old}} \leftarrow \pi_\theta$ and $V_{\phi_{old}} \leftarrow V_\phi$
 - 5: Estimate advantage $\hat{A}(s_t, a_t)$ through [21]
 - 6: Compute return $\hat{R}_t \leftarrow V_{\phi_{old}}(s_t) + \hat{A}(s_t, a_t)$
 - 7: **for** each training epoch **do**
 - 8: Compute \mathcal{L} as by (15)
 - 9: Update $\theta \leftarrow \theta - \lambda_\theta \nabla_\theta \mathcal{L}$, $\phi \leftarrow \phi - \lambda_\phi \nabla_\phi \mathcal{L}$
 - 10: **end for**
 - 11: **end while**
-

V. EXPERIMENTS

We conduct experiments to validate our method. In each episode, teams are randomly assigned to a side of the map with random initial postures, ensuring at least one of each aircraft type (F16 and A4) per team. Low-level agents follow the dynamics of \mathcal{G}_m and are trained in a 1-vs-1 setup, as observing additional entities may introduce noise and hinder precise maneuver control. High-level commanders are trained under \mathcal{G}_s dynamics in 3-vs-3 scenarios, with observations defined in Sec. IV-C. The termination condition β_c is either the destruction of an agent (by cannon or boundary exit) or expiration of the option duration, which is set to an upper bound of $\tau_k = 15$ low-level executions.

A rendered 3-vs-3 air combat situation of our environment is shown in Fig. 3a, with blue aircraft as the learning agents and red as opponents. The modularity of our environment allows to run any n -vs- m combat configuration. Fig. 3b illustrates trained agents during deployment on *VR-Forces*¹ (VR-F), a popular defense simulation tool. The realism achieved by JSBSim is further enhanced by VR-F through diverse scenarios and entities. After training agents in our JSBSim environment, their deployment is established through the *Distributed Interactive Simulation* [22], enabling real-time synchronization between JSBSim and VR-F over UDP/IP sockets. For the experiments discussed in this section, however, we only used our custom environment, which is much faster than VR-F. The complete integration with VR-F is ongoing and left as a future work.

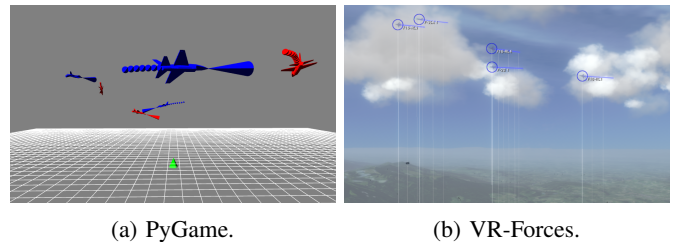


Fig. 3: Rendered air combat trajectories in (a) our custom environment using PyGame, and (b) VR-Forces when deployed.

¹mak.com/vr-forces.

A. Learning and Evaluation Parameters

Our training uses *Ray RLlib*. The SPO parameters are set as: learning rates $\lambda_\theta = \lambda_\phi = 10^{-4} \xrightarrow{15M} 10^{-5}$ (i.e., linearly decayed over 15M samples and then held constant), discount $\gamma = 0.995$, ratio $\epsilon = 0.25$, value coefficient $\kappa_v = 0.9$, entropy coefficient $\kappa_e = 0.05 \xrightarrow{3M} 0$, batch = 6'000 for π_c and 3'000 for π_h , with mini-batches of 256 each, and Adam as optimizer.

As SPO is similar to PPO, we compare these two *on-policy* algorithms using identical parameters. In addition, we include the *off-policy* algorithm *Soft Actor Critic* (SAC) [23], which is also used for aircraft control. Unlike SPO and PPO, which use entropy as a regularizer, SAC optimizes a maximum-entropy objective to encourage exploration using past data, making it more sample-efficient but also more sensitive to hyperparameter tuning, which can mislead policy optimization in complex control domains, as proven by [24]. We keep network architectures identical across all algorithms (see Sec. IV-E) and slightly adapt the standard SAC parameters from *Ray* to achieve best performance. Key changes include constant learning rates of $\lambda_\theta = \lambda_\phi = 3 \cdot 10^{-5}$, automatic target entropy tuning (matching the κ_e schedule), and soft update coefficient of 0.008, as SAC employs two critic networks to mitigate overestimation bias. Other algorithms, such as the popular reward-decomposition method QMIX [25], are omitted since our approach assigns per-agent rewards. Training on a 32-core 3.6 GHz CPU required around 10 h per initial π_c level, rising up to 30 h per remaining level and per commander π_h .

Evaluations are done for 1'000 episodes. A *win* is when all opponents are destroyed, *loss* if all agents are dead, and *draw* if none of the two cases occurs. Figures 4 and 5 show the mean rewards on y-axis over training samples on x-axis.

B. Low-Level Results

To have a consistent comparison across algorithms, we consider training on the starting level L1. The results are plotted in Fig. 4. SPO and PPO achieved 3 comparable performance, with SPO consistently outperforming PPO, while SAC performed worst. A reason for this is SAC's replay buffer that may store outdated transitions from obsolete opponent behaviors. Further, the shaping rewards (4), (7), and (9) may lead SPO and PPO to exploit these signals more directly, rather than SAC's exploration behavior, making the choice of *on-policy* algorithms reasonable. Comparing F16 to A4, a slightly more stable learning curve for F16 agents is observed, likely due to their higher maneuverability. As agents should only destroy opponents when in attack mode, we consider π_a of L4 in direct 1-vs-1 dogfight against its version at L3 and observe the following results: 64% win and 15% loss for π_a^f , 56% win and 19% loss for π_a^a , with remaining outcomes being draws.

C. High-Level Results

The high-level policies π_h are trained under CTDE using the MA-SPO algorithm, which we compare against MA-PPO. SAC is excluded since it only supports continuous actions, making it incompatible with the option space \mathcal{C}^i (Sec. IV-C). To emphasize the strength of our hierarchical scheme under

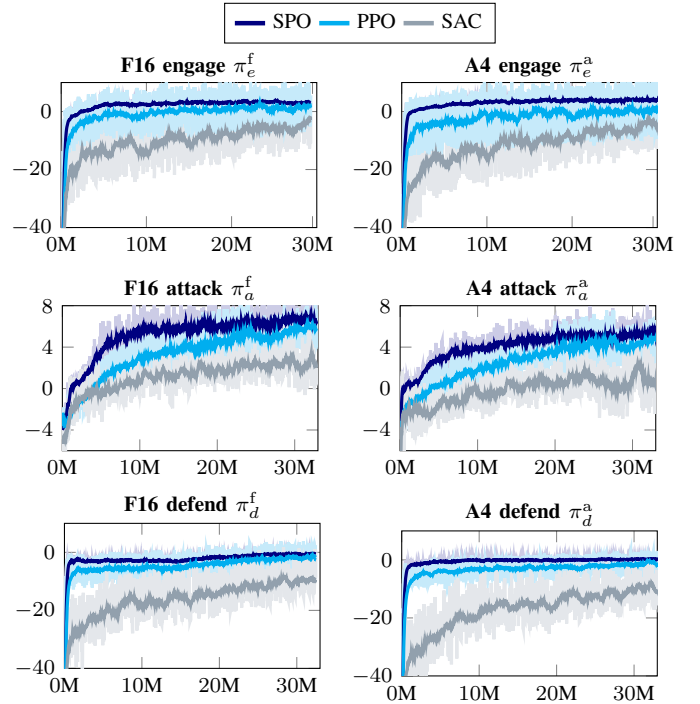


Fig. 4: Training results of all π_c on L1 across different tasks.

CL and the chosen network architecture, we use a *Fully Connected* (FC) network to train attack policies $\tilde{\pi}_a$ for F16 and A4 using SPO under full observability (denoted FC-SPO). Concretely, while hierarchical policies π_h^f and π_h^a incorporate pre-trained maneuver policies π_c , $\tilde{\pi}_a$ is to engage directly against opponents with mixed strategies (Sec. IV-D). The training results, shown in Fig. 5, report the mean values for both aircraft types. MA-SPO performs slightly better than MA-PPO, validating the effectiveness of our adaptation of SPO to MA-SPO, while $\tilde{\pi}_a$ trained with FC-SPO fails to achieve positive combat results. This indicates that *non-hierarchical* agents directly engaging strong opponents are likely to fail their mission, whereas our hierarchical agents effectively exploit strategic diversity through their maneuver options. While $\tilde{\pi}_a$ is *decentralized*, a fully *centralized* non-hierarchical model is omitted, as it is less common in MARL and scales poorly. FC-PPO performed similar to FC-SPO and is also excluded.

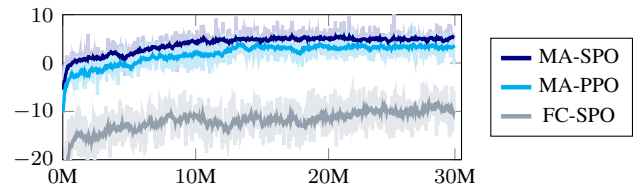


Fig. 5: Training of π_h through MA-SPO and MA-PPO and $\tilde{\pi}_a$ with FC-SPO against mixed strategy opponents (Sec. IV-D).

The evaluation results in Table I cover various *n-vs-m* scenarios, highlighting the flexibility of our approach via shared policies. We increase enemy aggressiveness by adjusting their

mixed strategy to select $\pi_a(70\%)$, $\pi_e(20\%)$, $\pi_d(10\%)$. The horizon is set 10 times higher as during training, as otherwise draws are mainly recorded in larger battle setups. Consistent with training results, we infer a clear superiority of MA-SPO and MA-PPO over FC-SPO. Our hierarchical MA-SPO agents show strong combat performance, achieving win rates above 80% even in competitive 10-vs-10 scenarios. Inspecting low-level policy activations reveals the team-level strategy, which is approximated by averaging the chosen options of both aircraft types, while per-agent-type strategies can be directly extracted from the outputs of π_h^f and π_h^a . As combat size increases, MA-SPO tends to become more cautious by favoring π_e and π_d , whereas MA-PPO acts slightly more aggressively by selecting π_a more often. A detailed analysis could examine under which conditions (e.g., distance d , aspect angle ω_a , etc.) each option π_c is chosen, revealing explanatory reasoning as similarly done in [26], but this lies beyond the scope of this work.

Combat	Model	Win	Draw	Loss	$\bar{\pi}_a/\bar{\pi}_a$	$\bar{\pi}_e$	$\bar{\pi}_d$
10-vs-10	MA-SPO	83%	6%	11%	72%	21%	7%
	MA-PPO	80%	7%	13%	61%	33%	6%
	FC-SPO	0%	6%	94%	100%	-	-
5-vs-5	MA-SPO	87%	4%	9%	77%	18%	5%
	MA-PPO	82%	6%	12%	59%	36%	5%
	FC-SPO	0%	5%	95%	100%	-	-
3-vs-3	MA-SPO	90%	3%	7%	76%	20%	4%
	MA-PPO	88%	3%	9%	56%	40%	4%
	FC-SPO	0%	2%	98%	100%	-	-

TABLE I: Inference results and average option activation frequencies ($\bar{\pi}_{a/e/d}$) for different scenarios and models. All values are averaged over 1'000 episodes and aircraft types.

VI. CONCLUSION

This work introduced a HMARL framework for competitive multi-agent air combat scenarios, combining realistic flight physics, heterogeneous dynamics, a structured training pipeline with reward shaping, CL and league-play, and the adapted training algorithm MA-SPO. Our results show that hierarchical agents acquire coordinated strategies and exhibit strong resilience compared to non-hierarchical baselines.

Nonetheless, some limitations remain. The reliance on fixed low-level controllers may restrict adaptability in highly dynamic or novel scenarios. While our setup focused on cannon-based close-range dogfights, further investigation is required to assess whether the hierarchical MA-SPO structure scales to more complex and long-range weapon systems.

Future research will aim to strengthen tactical decision-making by incorporating advanced planning methods such as LightZero [27]. In addition, our communication interface with VR-F enables direct interaction between human pilots and RL-controlled aircraft. By collecting explicit feedback from pilots, we plan to integrate imitation learning into the framework, fostering mixed human-RL teams and enabling new strategic maneuvers in operational training. Finally, interpretability and ethical considerations remain essential, as our approach aims to ensure human oversight and support trust and responsible deployment of intelligent agents in safety-critical domains.

REFERENCES

- [1] A. P. Pope, J. S. Ide, D. Mićović, H. Diaz, D. Rosenbluth, L. Ritholtz, J. C. Twedt, T. T. Walker, K. Alcedo, and D. Javorsek, "Hierarchical reinforcement learning for air combat," in *ICUAS*, 2021, pp. 275–284.
- [2] J. Berndt, "JSBSim: An Open Source Flight Dynamics Model in C++," in *Modeling and Simulation Technologies Conference*, 2004, p. 4923.
- [3] Z. Xie, Q. Zhang, F. Yang, M. Hutter, and R. Xu, "Simple Policy Optimization," in *ICML*, 2025.
- [4] P. R. Gorton, A. Strand, and K. Brathen, "A Survey of Air Combat Behavior Modeling using Machine Learning," *arXiv:2404.13954*, 2024.
- [5] D. Nanxun, W. Qinzhaoh, L. Qiang, and W. Wei, "Tactical Reward Shaping for Large-Scale Combat by Multi-Agent Reinforcement Learning," *Systems Engineering and Electronics*, vol. 35, pp. 1516–1529, 2024.
- [6] J. Yang, H. Zhang, H. Wang, X. Li, and C. Wang, "Heterogeneous unmanned swarm formation containment control based on reinforcement learning," *Aerospace Science and Technology*, vol. 150, p. 109186, 2024.
- [7] F. Jiang, M. Xu, Y. Li, H. Cui, and R. Wang, "Short-range air combat maneuver decision of UAV swarm based on multi-agent Transformer introducing virtual objects," *Applications of Artificial Intelligence*, 2023.
- [8] J. Hu and B. Sun, "ComSAC: Multi-Agent unmanned aerial vehicle swarm communication collaboration algorithm based on Soft Actor-Critic," in *ICAIRC*. IEEE, 2024, pp. 689–693.
- [9] Z. Zheng, C. Wei, and H. Duan, "UAV swarm air combat maneuver decision-making method based on multi-agent reinforcement learning and transferring," *Science China Information Sciences*, vol. 67, 2024.
- [10] Y. Zheng, B. Xin, B. He, and Y. Ding, "Mean policy-based proximal policy optimization for maneuvering decision in multi-UAV air combat," *Neural Computing and Applications*, vol. 36, pp. 19667–19690, 2024.
- [11] W.-r. Kong, D.-y. Zhou, Y.-j. Du, Y. Zhou, and Y.-y. Zhao, "Hierarchical Multi-Agent Reinforcement Learning for Multi-Aircraft Close-Range Air Combat," *IET Control Theory and Applications*, 2022.
- [12] J. Zhu, M. Kuang, W. Zhou, H. Shi, J. Zhu, and X. Han, "Mastering Air Combat Game with Deep Reinforcement Learning," *Defence Technology*, vol. 34, pp. 295–312, 2024.
- [13] J. Pang, J. He, N. M. A. A. Mohamed, C. Lin, Z. Zhang, and X. Hao, "A Hierarchical Reinforcement Learning Framework for Multi-UAV Combat using Leader-Follower Strategy," *Knowledge Systems*, 2025.
- [14] C. Yu, V. Akash, E. Vinitzky, J. Gao, Y. Wang, A. Bayen, and Y. Wu, "The Surprising Effectiveness of PPO in Cooperative Multi-Agent Games," in *NeurIPS*, vol. 35, 2022.
- [15] M. L. Littman, "Markov Games as a Framework for Multi-Agent Reinforcement Learning," in *ICML*. Elsevier, 1994, pp. 157–163.
- [16] A. Barto and S. Mahadevan, "Recent Advantages in Hierarchical Reinforcement Learning," *Discrete Event Dynamic Systems*, pp. 41–77, 2003.
- [17] K. Tanaka and K. Wakuta, "Semi-Markov Games," *Projecteuclid*, 1976.
- [18] A. Selmonaj, O. Szehr, G. Del Rio, A. Antonucci, A. Schneider, and M. Rügsegger, "Hierarchical Multi-Agent Reinforcement Learning for Air Combat Maneuvering," in *ICMLA*, 2023, pp. 1031–1038.
- [19] V. R. Konda and J. N. Tsitsiklis, "Actor-Critic Algorithms," in *NeurIPS*. The MIT Press, 1999, pp. 1008–1014.
- [20] R. Lowe, Y. I. Wu, A. Tamar, J. Harb, O. Pieter Abbeel, and I. Mordatch, "Multi-Agent Actor-Critic for Mixed Cooperative-Competitive Environments," in *NeurIPS*, vol. 30, 2017, pp. 6379–6390.
- [21] J. Schulman, P. Moritz, S. Levine, M. Jordan, and P. Abbeel, "High-dimensional continuous control using generalized advantage estimation," *arXiv:1506.02438*, 2015.
- [22] IEEE, "Standard for information technology – protocols for distributed interactive simulation applications," Tech. Rep. IEEE Std 1278, 1993.
- [23] T. Haarnoja, A. Zhou, P. Abbeel, and S. Levine, "Soft Actor-Critic: Off-Policy Maximum Entropy Deep Reinforcement Learning with a Stochastic Actor," in *ICML*, 2018, pp. 1861–1870.
- [24] R. Zhang, Y.-C. Chang, and S. Gao, "When Maximum Entropy Misdreads Policy Optimization," in *ICML*, 2025.
- [25] T. Rashid, M. Samvelyan, C. Schroeder, G. Farquhar, J. Foerster, and S. Whiteson, "QMIX: Monotonic Value Function Factorisation for Deep Multi-Agent Reinforcement Learning," in *ICML*, 2018, pp. 4295–4304.
- [26] A. Selmonaj, A. Antonucci, A. Schneider, M. Rügsegger, and M. Sommer, "Explainability in Multi-Agent Reinforcement Learning for Air Combat Tactics," *M&S as Enabler for Digital Transformation in NATO and Nations*, vol. 217, 2024.
- [27] Y. Niu, Y. Pu, Z. Yang, X. Li, T. Zhou, J. Ren, S. Hu, H. Li, and Y. Liu, "LightZero: A Unified Benchmark for Monte Carlo Tree Search in General Sequential Decision Scenarios," *NeurIPS*, vol. 36, 2024.